Journal of Applied Research and Technology

www.jart.icat.unam.mx

Journal of Applied Research and Technology 24 (2026) 122-131

Original

Controlling the Primary Resonance Vibrations of a Hybrid Rayleigh-Van der Pol-Duffing Oscillator Using Negative Cubic Velocity Feedback

Osama M. Khaled[1] · Yasser A. Amer[2]
Abdullah Reda[3] · Mansour N. Abd El-Salam[4*]

[1]*Department of Mathematical and Computer Science, Faculty of Science, Port Said University, Port Said, Egypt*
[2]*Mathematics Department, Science Faculty, Zagazig University, Zagazig, Egypt*
[3]*Department of Mathematics, Saxony Egypt University for Applied Science and Technology, Cairo 11511, Egypt*
[4]*Department of Basic Sciences, Common First Year Deanship, King Saud University, Riyadh 12373, Saudi Arabia*

Received: 02 09 2024; Accepted: 16 02 2025
Available: 28 02 2026

Abstract: This study aims to suppress vibrations in hybrid Rayleigh-Van der Pol-Duffing oscillators by employing negative cubic velocity feedback control. The system's behavior is analyzed using the multiple-scales method to derive solutions up to the second-order approximation. The effect of negative cubic velocity feedback is specifically examined under primary resonance conditions. The influence of various system parameters is explored numerically using MATLAB. The findings reveal a strong correlation between the approximate analytical solutions and numerical results, confirming the effectiveness of the proposed approach.

Keywords: Negative cubic velocity feedback, multiple-scales method, primary resonance, stability fixed point

*Corresponding author.
E-mail address: mansour.naserallah@yahoo.com (M.N. Abd El-Salam).
Peer Review under the responsibility of Universidad Nacional Autónoma de México.

1. Introduction

In many applications in the physical sciences and engineering, one of the most significant models is the duffing oscillator. It is utilized in optical stability, plasma oscillations, electric circuits, and buckling beams, as demonstrated by Siewe et al. (2006), Trueba et al. (2003). Huang (2018) suppressed the Van der Pol oscillator's vibrations using a nonlinear time-delayed feedback controller, and the impact of the feedback gain at the bifurcation point was evaluated. Amer et al. (2022) The vibration analysis and dynamic responses of a hybrid Rayleigh-Van der Pol-Duffing oscillator were studied using a proportional-derivative (PD) controller. The average method was employed to obtain the approximate solution of the vibrating system. Barron (2016) provided a numerical explanation for the behavior of a ring of coupled Van der Pol oscillators' stable and unstable responses. Barron showed that the Van der Pol oscillator's amplitude rises when the stability requirements are not satisfied. Comprehensive bifurcation investigations of the Van der Pol, Duffing, and Rayleigh oscillators were conducted by Kumar et al. (2016), Kumar et al. (2017), Kumar et al. (2018), revealing and clarifying their modulation. Amer et al. (2020b) used two separate time delays, one for displacement and the other for velocity, to control the vibration of the oscillator. It was discovered that the vibrations were reduced by nearly 94% compared to their value without control, and the effectiveness of the time delay controller was approximately 17. Kandil et al. (2022) applied negative cubic velocity feedback control to manage, reduce, and stabilize a coupled pitch-roll ship model. Kamel (2009) studied multi-force stimulated coupled Van der Pol oscillators. He examined the stability of this system at two notable resonances using frequency response equations. Sayed et al. (2018) modulated the harmonic and parametric force-induced vibrations of the Van der Pol oscillator utilizing negative acceleration feedback control.

A tuned damper, or passive control, was used by Wang et al. (2018) to suppress the Van der Pol oscillator's vibrations. Through time-delay analysis, El-Sayed (2021) demonstrated the effectiveness of positive position feedback (PPF) controllers with time delays in reducing vibrations in linked Van der Pol oscillators. Amer et al. (2020a) investigated the stability of a one-degree-of-freedom Rayleigh-Van der Pol-Duffing oscillator with cubic nonlinear terms and an external force, incorporating a nonlinear integral positive position feedback controller. Hamed et al. (2020) used a nonlinear proportional-derivative controller (NPD) to reduce vibrations in a vertical conveyor system. The amplitudes of the two modes were reduced by roughly 95.33% and 82.45% compared to their values before using the NPD control. Amer et al. (2020a) investigated the numerical and stability aspects of a hybrid Rayleigh-Van der Pol-Duffing oscillator controlled by nonlinear integral positive position feedback (NIPPF). When Sadeghi et al. (2021) investigated particle swarm optimization (PSO), they found that adding more terms to the selected trial functions could reduce inaccuracy even more. In this paper, the negative cubic velocity feedback controller is used to suppress the vibrations of a hybrid Rayleigh-Van der Pol-Duffing oscillator excited by an external force. We use the perturbation technique to solve the hybrid Rayleigh-Van der Pol-Duffing oscillator up to the second approximation. Numerically, we investigate the behavior of the vibrating system before and after using the negative cubic velocity feedback control. An illustration is provided to demonstrate the effects of various parameters and negative cubic velocity on the main system. Finally, there is a good agreement between the approximate and numerical solutions.

2. Mathematical Formulation

Kumar et al. (2016) introduced the hybrid Rayleigh-Van der Pol-Duffing oscillator with one degree of freedom as follows:

$$\frac{d^2q}{dt^2}+\omega^2 q-2\mu\omega\frac{dq}{dt}+\alpha_1 q^3+\alpha_2\left(\frac{dq}{dt}\right)^2 +\alpha_3\left(\frac{dq}{dt}\right)^3+\beta_1\left(\frac{dq}{dt}\right)q^2+\beta_2\left(\frac{dq}{dt}\right)^2 q^2+\beta_3 q^5=0 \quad (1)$$

To suppress the vibrations of the investigated system, a negative cubic velocity feedback controller will be used, as shown in Figure 1, which presents the closed-loop of the controlled system. Then Equation (1) is written as follows:

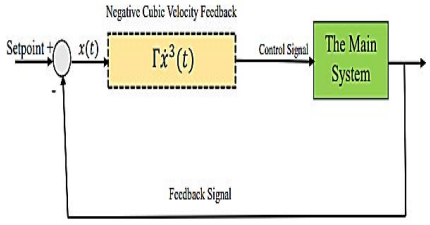

Figure 1. The Closed-loop control system.

$$\frac{d^2q}{dt^2}+\omega^2 q-2\varepsilon\hat{\mu}\omega\frac{dq}{dt}+\varepsilon\hat{\alpha}_1 q^3 +\varepsilon\hat{\alpha}_2\left(\frac{dq}{dt}\right)^2+\varepsilon\hat{\alpha}_3\left(\frac{dq}{dt}\right)^3+\varepsilon^2\hat{\beta}_1\left(\frac{dq}{dt}\right)q^2 +\varepsilon^2\hat{\beta}_2\left(\frac{dq}{dt}\right)^2 q^2+\varepsilon^2\hat{\beta}_3 q^5=\varepsilon^2\hat{f}\cos(\Omega t) -\varepsilon^2\hat{\Gamma}\left(\frac{dq}{dt}\right)^3 \quad (2)$$

Where the hybrid Rayleigh-Van der Pol-Duffing oscillator's position is represented by q. We used $\mu=\varepsilon\hat{\mu}$ as the hybrid Rayleigh-Van der Pol-Duffing oscillator's damping coefficient. The coefficients of nonlinear terms are represented by $\alpha_i=\varepsilon\hat{\alpha}_i$, $\beta_i=\varepsilon^2\hat{\beta}_i$;$(i=1,2,3)$. The Van der Pol oscillator's frequency response is ω. The excitation's frequency and amplitude are $\Omega, f=\varepsilon^2\hat{f}$ the negative cubic velocity feedback's coefficient is represented by $\Gamma=\varepsilon^2\hat{\Gamma}$.

In Equation (2), $\frac{d^2q}{dt^2}$ presents the inertial term, and $\omega^2 q$ represents the linear restoring force. The constant ω is related to the natural frequency of the oscillator. The energy dissipation in the system given by $\varepsilon\,\mu\frac{dq}{dt}$. The parameter is ε a small perturbation parameter, and μ is the damping coefficient. $f\ cos\ (\Omega t)$ is a periodic forcing term representing an external periodic driving force with amplitude f, and angular frequency Ω. For more damping, the negative cubic velocity feedback $\Gamma\,\dot{x}^3$ presented as an active control.

3. Perturbation Analysis

Utilizing the multiple-scales method Nayfeh (1978) up to the second approximation to determine the solution of the controlled system presented in Equation (2) as follows:

$$\mathrm{q}(t;\varepsilon)=q_o(T_2,T_1,T_0)+\varepsilon q_1(T_2,T_1,T_0)+\varepsilon^2 q_2(T_2,T_1,T_0) \quad (3)$$

Where $\mathrm{T}_0=t$, $\mathrm{T}_1=\varepsilon t$, and $\mathrm{T}_2=\varepsilon t^2$ are the time scales. We will convert the derivatives into the following form:

$$\left.\begin{aligned}\frac{d}{dt}&=D_o+\varepsilon D_1+\varepsilon^2 D_2+\ldots\\ \frac{d^2}{dt^2}&=D_o{}^2+2\varepsilon D_o D_1+\varepsilon^2(D_1^2+2D_oD_2)+\ldots\end{aligned}\right\} \quad (4)$$

where $D_n=\frac{\partial}{\partial T_n}$ (n=0, 1, 2). Substituting Equations (3) and (4) into Equation (2) and then, equating the coefficients of the same power of ε.

$$O(\varepsilon^0):$$

$$(D_o{}^2+\omega^2)\,\mathrm{q}_o=0 \quad (5)$$

$$O(\varepsilon):$$

$$(D_0^2+\omega^2)\,\mathrm{q}_1=-2D_1(D_0q_0)+2\hat{\mu}\omega(D_0q_0)-\hat{\alpha}_1q_0^3-\hat{\alpha}_2(D_0q_0)^2-\hat{\alpha}_3(D_0q_0)^3 \quad (6)$$

$$O(\varepsilon^2):$$

$$(D_0^2+\omega^2)\,\mathrm{q}_2=-2D_0D_1q_1-2D_1^2q_0-2D_0D_2q_0 +2\hat{\mu}\omega(D_0q_1+D_1q_0)-3\hat{\alpha}_1q_0^2q_1-2\hat{\alpha}_2D_0q_1(D_0q_0) -2\hat{\alpha}_2D_1q_0(D_0q_0)-3\hat{\alpha}_3D_0q_1(D_0q_0)^2 -3\hat{\alpha}_3D_1q_0(D_0q_0)^2-\hat{\beta}_1q_0^2(D_0q_0) -\hat{\beta}_2q_0^2(D_0q_0)^2-\hat{\beta}_3q_0^5+\hat{f}\cos(\Omega t)-\hat{\Gamma}(D_0q_0)^3 \quad (7)$$

By solving the homogeneous differential Equation (5), the solution takes the following form:

$$q_o(T_2,T_1,T_0)=A(T_2,T_1)e^{i\omega T_0}+\bar{A}(T_2,T_1)e^{-i\omega T_0} \quad (8)$$

Where A is a complex function in T_1, T_2 and $\bar{A}$ is its conjugate function. By using Equation (8) to evaluate all terms on the right-hand side of Equation (6),

$$(D_0^2+\omega^2)\,\mathrm{q}_1=(-2i\omega D_1A+2i\hat{\mu}\omega^2A-3\hat{\alpha}_1A^2\bar{A} -3i\hat{\alpha}_3\omega^3A^2\bar{A})e^{i\omega T_0}+\hat{\alpha}_2\omega^2A^2e^{2i\omega T_0} +(i\hat{\alpha}_3\omega^3A^3-\hat{\alpha}_1A^3)e^{3i\omega T_0}-2\hat{\alpha}_2\omega^2A\bar{A}+cc \quad (9)$$

Such that cc are the complex conjugate terms. The secular terms are the terms that make the solutions of the Equation (9) approach infinity, and they occur in cases of resonance.

$$-2i\omega D_1 A+2i\hat{\mu}\omega^2 A-3\hat{\alpha}_1 A^2\overline{A}-3i\hat{\alpha}_3\omega^3 A^2\overline{A}=0 \tag{10}$$

After eliminating these terms, the first approximation can be written as:

$$q_1(T_2,T_1,T_0)=-\frac{\hat{\alpha}_2 A^2}{3}e^{2i\omega T_0}$$
$$-\frac{(i\hat{\alpha}_3\omega^3 A^3-\hat{\alpha}_1 A^3)}{8\omega^2}e^{3i\omega T_0}-2\hat{\alpha}_2 A\overline{A}+cc. \tag{11}$$

The solvability conditions from the first approximation were obtained from Equation (10) as follows:

$$\begin{cases} D_1 A=\hat{\mu}\omega A+\dfrac{3i\,\hat{\alpha}_1 A^2\overline{A}}{2\omega}-\dfrac{3\hat{\alpha}_3\omega^2 A^2\overline{A}}{2} \\ D_1\overline{A}=\hat{\mu}\omega\overline{A}-\dfrac{3i\,\hat{\alpha}_1\overline{A}^2 A}{2\omega}-\dfrac{3\hat{\alpha}_3\omega^2\overline{A}^2 A}{2} \end{cases} \tag{12}$$

To evaluate the second approximation, we will insert Equations (8) and (11) into Equation (7) as follows:

$$(\mathrm{D}_0^2+\omega^2)q_2=(13\hat{\alpha}_1\hat{\alpha}_3-2i\omega^3\hat{\alpha}_2\hat{\alpha}_3-2\hat{\beta}_2\omega^2)A^2\overline{A}^2$$
$$+(\frac{-3A^3\overline{A}^2\hat{\alpha}_1^2}{8\omega^2}+\frac{3i\omega A^3\overline{A}^2\hat{\alpha}_1\hat{\alpha}_3}{2}+\frac{9\omega^4 A^3\overline{A}^2\hat{\alpha}_3^2}{8}$$
$$-10\hat{\beta}_3 A^3\overline{A}^2-3\omega^2\hat{\alpha}_3 D_1 A^2\overline{A}-3i\hat{\Gamma}\omega^3 A^2\overline{A}$$
$$+\frac{4\omega^2 A^2\overline{A}\hat{\alpha}_2^2}{8}-i\hat{\beta}_1\omega A^2\overline{A}-2\mathrm{D}_1^2 A+2\hat{\mu}\omega D_1 A$$
$$-2i\omega D_2 A)e^{i\omega T_0}+(7.25A^3\overline{A}\hat{\alpha}_1\hat{\alpha}_2+\frac{19i\omega^3 A^3\overline{A}\hat{\alpha}_2\hat{\alpha}_3}{4}$$
$$-\frac{2i\omega\hat{\alpha}_2 D_1 A^2}{3}-\frac{4i\omega^2\mu\hat{\alpha}_2 A^2}{3})e^{2i\omega T_0}+\frac{\hat{f}}{2}e^{i\Omega T_0}$$
$$+(\frac{-3A^4\overline{A}\hat{\alpha}_1^2}{4\omega^2}-\frac{3i\omega A^4\overline{A}\hat{\alpha}_1\hat{\alpha}_3}{2}-\frac{9\omega^4 A^4\overline{A}\hat{\alpha}_3^2}{4}$$
$$-5\hat{\beta}_3 A^4\overline{A}-\frac{3i\hat{\alpha}_1 D_1 A^3}{4\omega}+\frac{9\omega^2\hat{\alpha}_3 D_1 A^3}{4}+i\hat{\Gamma}\omega^3 A^3$$
$$+\frac{3i\hat{\alpha}_1\hat{\mu}A^3}{4}+\frac{3\omega^3\hat{\alpha}_3\hat{\mu}A^3}{4}-\frac{4\omega^2 A^3\hat{\alpha}_2^2}{3}-i\hat{\beta}_1\omega A^3)e^{3i\omega T_0}$$
$$+(1.75A^4\hat{\alpha}_1\hat{\alpha}_2-\frac{11i\omega^3 A^4\hat{\alpha}_2\hat{\alpha}_3}{4}+\hat{\beta}_2\omega^2 A^4)e^{4i\omega T_0}$$
$$(\frac{-3A^5\hat{\alpha}_1^2}{8\omega^2}+\frac{3i\omega A^5\hat{\alpha}_1\hat{\alpha}_3}{2}+\frac{9\omega^4 A^5\hat{\alpha}_3^2}{8}-\hat{\beta}_3 A^5)e^{5i\omega T_0}+c.c. \tag{13}$$

After eliminating the secular terms from Equation (13), the second approximation can be written as:

$$(\mathrm{D}_0^2+\omega^2)\mathrm{q}_2=\mathrm{E}_0(T_0,T_1,T_2)+\mathrm{E}_1(T_0,T_1,T_2)e^{2i\omega T_0}$$
$$+\mathrm{E}_2(T_0,T_1,T_2)e^{3i\omega T_0}+\mathrm{E}_3(T_0,T_1,T_2)e^{4i\omega T_0}$$
$$+\mathrm{E}_4(T_0,T_1,T_2)e^{5i\omega T_0}+E_5(T_0,T_1,T_2)e^{i\Omega T_0}+cc. \tag{14}$$

Where $E_j, j=0,1,\ldots,5$ are included in the Appendix.

4. The Periodic Solution

In this part, we introduce the detuning parameter σ to evaluate the stability of the investigated system in the primary resonance case:

$$\Omega=\omega+\varepsilon\sigma \tag{15}$$

Substituting Equations (15) and (12) into Equation (13) and eliminating all secular terms yields:

$$D_2 A=-\frac{33iA^3\overline{A}^2\hat{\alpha}_1^2}{16\omega^3}+\frac{15A^3\overline{A}^2\hat{\alpha}_1\hat{\alpha}_3}{2}-\frac{9i\omega^3\hat{\alpha}_3^2 A^3\overline{A}^2}{16}$$
$$+\frac{5i\hat{\beta}_3 A^3\overline{A}^2}{\omega}-\frac{3\hat{\Gamma}\omega^2 A^2\overline{A}}{2}-\frac{9\hat{\mu}\hat{\alpha}_1 A^2\overline{A}}{2\omega}-\frac{2i\omega\hat{\alpha}_2^2 A^2\overline{A}}{3}$$
$$-\frac{\hat{\beta}_1 A^2\overline{A}}{2}-\frac{i\hat{f}}{4\omega}e^{i\sigma T_1} \tag{16}$$

According to the definition of the first derivative presented in Equation (4),

$$\frac{dA}{dt}=\varepsilon D_1 A+\varepsilon^2 D_2 A \tag{17}$$

Inserting Equations (12) and (16) into Equation (17),

$$\frac{dA}{dt}=\varepsilon\left(\hat{\mu}\omega A+\frac{3i\hat{\alpha}_1 A^2\overline{A}}{2\omega}-\frac{3\hat{\alpha}_3\omega^2 A^2\overline{A}}{2}\right)$$
$$+\varepsilon^2\left(\begin{array}{l}-\dfrac{33iA^3\overline{A}^2\hat{\alpha}_1^2}{16\omega^3}+\dfrac{15A^3\overline{A}^2\hat{\alpha}_1\hat{\alpha}_3}{2}-\dfrac{9i\omega^3\hat{\alpha}_3^2 A^3\overline{A}^2}{16} \\ +\dfrac{5i\hat{\beta}_3 A^3\overline{A}^2}{\omega}-\dfrac{3\hat{\Gamma}\omega^2 A^2\overline{A}}{2}-\dfrac{9\hat{\mu}\hat{\alpha}_1 A^2\overline{A}}{2\omega} \\ -\dfrac{2i\omega\hat{\alpha}_2^2 A^2\overline{A}}{3}-\dfrac{\hat{\beta}_1 A^2\overline{A}}{2}-\dfrac{i\hat{f}}{4\omega}e^{i\sigma T_1}\end{array}\right) \tag{18}$$

Returning to the parameters of the main system as follows:

$$\frac{dA}{dt}=\left(\mu\omega A+\frac{3i\alpha_1A^2\bar{A}}{2\omega}-\frac{3\alpha_3\omega^2A^2\bar{A}}{2}\right)+\left(\begin{array}{l}-\frac{33iA^3\bar{A}^2\alpha_1^2}{16\omega^3}+\frac{15A^3\bar{A}^2\alpha_1\alpha_3}{2}\\-\frac{9i\omega^3\alpha_3^2A^3\bar{A}^2}{16}+\frac{5i\beta_3A^3\bar{A}^2}{\omega}-\frac{3\Gamma\omega^2A^2\bar{A}}{2}\\-\frac{9\mu\alpha_1A^2\bar{A}}{2\omega}-\frac{2i\omega\alpha_2^2A^2\bar{A}}{3}-\frac{\beta_1A^2\bar{A}}{2}-\frac{if}{4\omega}e^{i\sigma T_1}\end{array}\right) \quad (19)$$

By converting function A to its polar form,

$$\begin{cases}A(t)=\frac{1}{2}a(t)e^{i\theta(t)}\\\frac{dA}{dt}=\frac{1}{2}\left(\dot{a}+i\,a\,\dot{\theta}\right)e^{i\theta}\end{cases} \quad (20)$$

Where the motion's steady-state phase is θ and its amplitude is presented by a. Inserting Equation (20) into Equation (19) and equating the real and imaginary parts, we obtain:

$$\dot{a}=\mu\omega a-\frac{3\omega^2\alpha_3}{8}a^3+\frac{15\alpha_1\alpha_3}{32}a^5-\frac{3\Gamma\omega^2}{8}a^3-\frac{9\alpha_1\mu}{8\omega}a^3-\frac{\beta_1}{8}a^3+\frac{f}{2\omega}\sin\varphi \quad (21)$$

$$a\dot{\varphi}=\sigma a-\frac{3\alpha_1}{8\omega}a^3+\frac{33\alpha_1^2}{256\omega^3}a^5+\frac{9\omega^3\alpha_3^2}{256}a^5-\frac{5\beta_3}{16\omega}a^5+\frac{\omega\alpha_2^2}{6}a^3+\frac{f}{2\omega}\cos\varphi \quad (22)$$

Where, $\varphi=\sigma T_1-\theta$.

5. Fixed-Point Solution

The steady-state amplitude and phase angle of the vibrating system can be obtained by putting $\dot{a}=\dot{\varphi}=0$ which means that, $\dot{\theta}=\sigma$. So, we will obtain the following nonlinear algebraic system of equations

$$\frac{f}{2\omega}\sin\varphi=\frac{3\omega^2\alpha_3}{8}a^3+\frac{3\Gamma\omega^2}{8}a^3+\frac{9\alpha_1\mu}{8\omega}a^3+\frac{\beta_1}{8}a^3-\mu\omega a-\frac{15\alpha_1\alpha_3}{32}a^5 \quad (23)$$

$$\frac{f}{2\omega}\cos\varphi=\frac{3\alpha_1}{8\omega}a^3+\frac{5\beta_3}{16\omega}a^5-\frac{\omega\alpha_2^2}{6}a^3-\frac{33\alpha_1^2}{256\omega^3}a^5-\frac{9\omega^3\alpha_3^2}{256}a^5-\sigma a \quad (24)$$

By squaring each of Equations (23) and (24) and then adding, we get

$$\frac{f^2}{4\omega^2}=\left(\frac{3\omega^2\alpha_3}{8}a^3+\frac{3\Gamma\omega^2}{8}a^3+\frac{9\alpha_1\mu}{8\omega}a^3+\frac{\beta_1}{8}a^3-\mu\omega a-\frac{15\alpha_1\alpha_3}{32}a^5\right)^2+\left(\frac{3\alpha_1}{8\omega}a^3+\frac{5\beta_3}{16\omega}a^5-\frac{\omega\alpha_2^2}{6}a^3-\frac{33\alpha_1^2}{256\omega^3}a^5-\frac{9\omega^3\alpha_3^2}{256}a^5-\sigma a\right)^2 \quad (25)$$

The stability of the nonlinear differential Equations (21) and (22) is analyzed by resorting to the first (indirect) method of Lyapunov as follows:

$$\begin{bmatrix}\dot{a}\\\dot{\varphi}\end{bmatrix}=\begin{bmatrix}\chi_{11}&\chi_{12}\\\chi_{21}&\chi_{22}\end{bmatrix}\begin{bmatrix}a\\\varphi\end{bmatrix} \quad (26)$$

Where,

$$\begin{cases}\chi_{11}=\frac{\partial\dot{a}}{\partial a}=\mu\omega-\frac{9\omega^2\alpha_3}{8}a^2+\frac{75\alpha_1\alpha_3}{32}a^4-\frac{9\Gamma\omega^2}{8}a^2-\frac{27\alpha_1\mu}{8\omega}a^2-\frac{3\beta_1}{8}a^2\\\chi_{12}=\frac{\partial\dot{a}}{\partial\varphi}=\frac{f}{2\omega}\cos\varphi\\\chi_{21}=\frac{\partial\dot{\varphi}}{\partial a}=\frac{\sigma}{2}-\frac{9\alpha_1}{8\omega}a+\frac{165\alpha_1^2}{256\omega^3}a^3+\frac{45\omega^3\alpha_3^2}{256}a^3-\frac{25\beta_3}{16\omega}a^3+\frac{\omega\alpha_2^2}{2}a\\\chi_{22}=\frac{\partial\dot{\varphi}}{\partial\varphi}=-\frac{f}{2\omega a}\sin\varphi\end{cases} \quad (27)$$

To study the stability of the system in Equation (26), we must solve the following equation to obtain its eigenvalues, λ,

$$\begin{vmatrix} \chi_{11}-\lambda & \chi_{12} \\ \chi_{21} & \chi_{22}-\lambda \end{vmatrix} = 0 \quad (28)$$

By resolving Equation (28), we will have a polynomial of the second degree in λ as

$$\lambda^2 - (\chi_{11}+\chi_{22})\lambda + \chi_{11}\chi_{22} - \chi_{21}\chi_{12} = 0 \quad (29)$$

The stability criteria might be written as

$$\chi_{11}+\chi_{22} \succ 0, \qquad \chi_{11}\chi_{22} - \chi_{21}\chi_{12} \succ 0 \quad (30)$$

The following section presents a numerical investigation of the theoretical results discussed earlier.

6. Numerical Results

This section presents the numerical and approximate solutions for the hybrid Rayleigh-Van der Pol-Duffing oscillator, both before and after applying the negative cubic velocity feedback controller at the primary resonance condition($\Omega = \omega$). The investigation focuses on the impact of various parameters on the steady-state amplitudes of the oscillator.

6.1 Time History

To observe the behavior of the hybrid Rayleigh-Van der Pol-Duffing oscillator before and after applying the negative cubic velocity feedback control, we investigated the primary resonance case. The time histories of the main system for the open and closed loops are shown in Figures 1a and 1b. The numerical solution is presented by the solid red line, while the approximate solution is plotted by the dotted blue line. The regulated system exhibited an amplitude reduction of approximately 83% relative to the uncontrolled amplitude. The aforementioned result indicates that the control's performance ($E_a = \frac{amplitude\ without\ controller}{amplitude\ with\ controller}$) is equal to 6. The convention of approximating solutions using the multiple-scales approach and numerical solutions using the RK-4 method was also discussed in these figures. From Figure 2, the appropriate values for the cubic velocity coefficient G where $\Gamma = 10$.

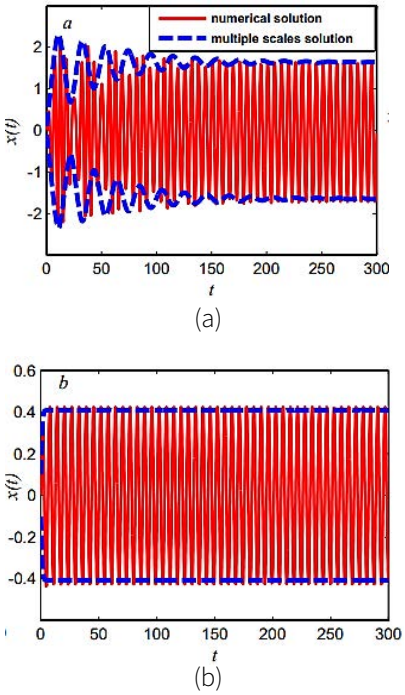

Figure 1. The primary amplitude of the system is (a) without the controller and (b) with the controller.

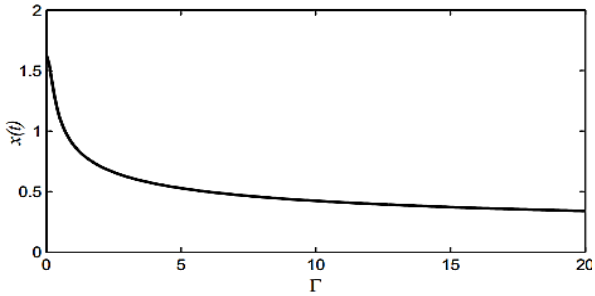

Figure 2. The effect of the negative cubic velocity influence coefficient Γ when f=0.5.

6.2 Response Curves

In this section, the frequency response curves are plotted for $-10 \le \sigma \le 10$. The impact of the cubic velocity coefficient Γ, the natural frequency ω, the damping coefficient μ, and the external force f are studied. The numerical solution of Equation (24) obtained for the amplitude of the hybrid Rayleigh–Van der Pol–Duffing oscillator via the detuning parameter σ which, is represented by one peak. The solid line expresses the stable solution, while the dashed line expresses the unstable solution as shown in Figure 3. From this figure, the stable solution is presented in the region $-7.38 \le \sigma \le 7.38$

and the unstable solution is presented in two regions $-10 \le \sigma \le -7.38$ and $7.38 \le \sigma \le 10$. In the stable region, we selected two points B (-3.43, 0.07), and C (5.4, 0.04) in the unstable region, we selected another two points A (-8.92, 0.02), D (7.86, 0.03). At each point, we determined the eigenvalues from Equation (25) and investigated stability conditions as listed in Table 1. From this table, the solution is stable at B, and C but unstable at A and, D which is in agreement with our numerical investigation presented in Figure 3. The of the external force and the coefficient of negative cubic feedback controller was studied in Figures 4 and 5. These graphs show that the controlled system's amplitude increases with the external force but decreases with the coefficient of negative cubic feedback and that the unstable regions vanish for the highest theme values. Figures 6 and 7 illustrate how the amplitude decreases with the natural frequency and damping coefficient. At the lowest theme values, the unstable regions vanish.

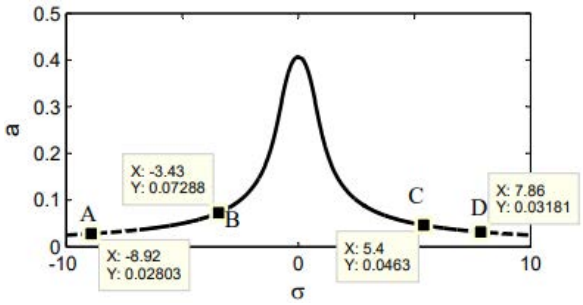

Figure 3. The response curve of the controlled system at $\Gamma = 10$.

Table 1. Determined eigenvalues of some selected points shown in Figure 3.

Points (σ, a)	Eigenvalues $\lambda_{1,2} = \alpha + i\xi$	Sign real part α	Classify of Solution
A (-8.92,0.02)	$\lambda_{1,2} = 0.069 \pm 0.0299i$	Positive	Unstable
B (-3.43,0.07)	$\lambda_{1,2} = -0.0268 \pm 0.0529i$	Negative	Stable
C (5.4,0.04)	$\lambda_{1,2} = -0.002 \pm 0.0418i$	Negative	Stable
D (7.86,0.03)	$\lambda_{1,2} = 0.032 \pm 0.0365i$	Positive	Unstable

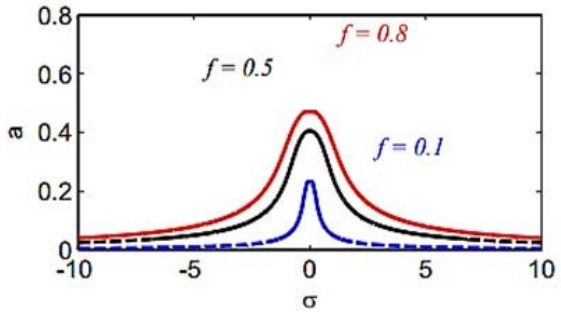

Figure 4. Response curves for different values of the external force.

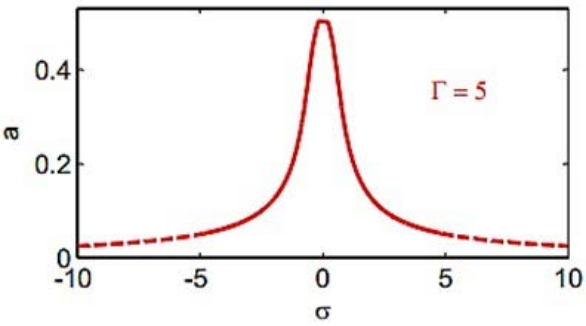

(a)

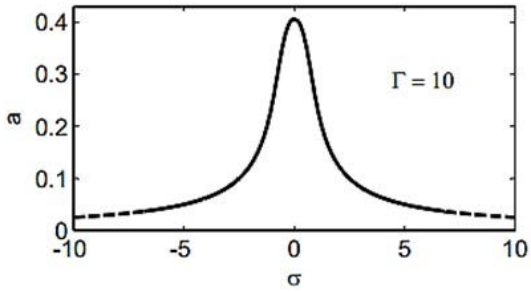

(b)

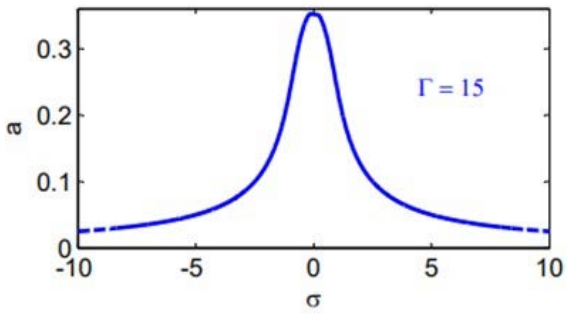

(c)

Figure 5.Response curves to different values of the control gain: (a) Γ=5; (b) Γ= 10; (c) Γ=15.

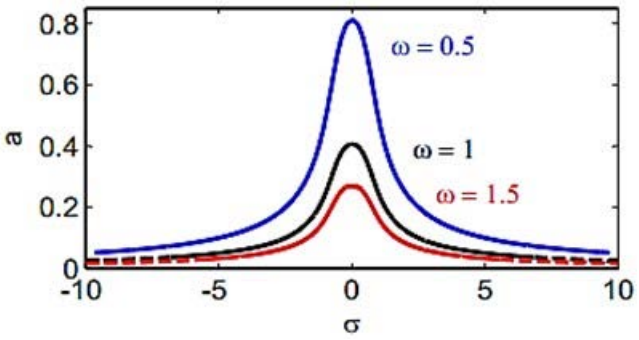

Figure 6. The response curves to different values of natural frequency.

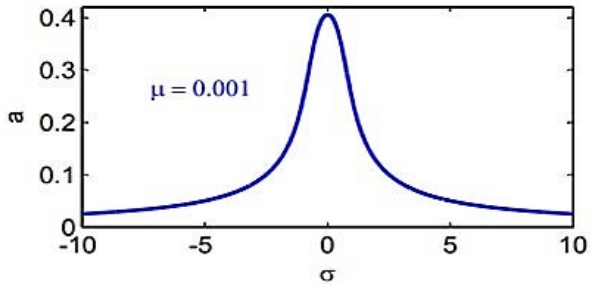

(a)

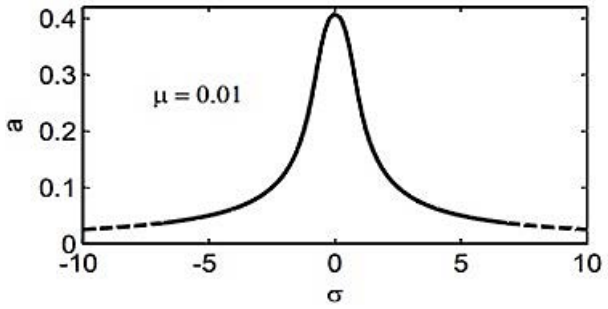

(b)

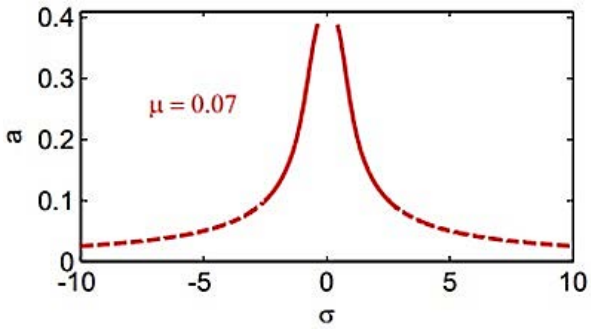

(c)

Figure 7. Response curves for different values of the damping coefficient: (a): μ=0.001; (b) μ=0.01; (c) μ=0.07.

7.Conclusion

The oscillator is one of the most important models in physics and engineering, where the Duffing equation finds many uses. It is used in optical stability, plasma oscillations, electric circuits, and buckling beams. The Rayleigh-Van der Pol-Duffing oscillator's dynamic responses and vibration analysis were examined in the presence of an external force. We employed the multiple-scales approach to obtain the vibrating system's approximate solution. To reduce the hybrid Rayleigh-Van der Pol-Duffing oscillator's large amplitudes, the negative cubic velocity control feedback was incorporated. The multiple-scale method yields the analytical solution up to the second approximation. The amplitude of the managed system was approximately 83% less than that of the uncontrolled system. This indicates that the performance of the control E_a is rough. According to the study presented, we can conclude the following:

i. As the external force increases, so does the system's amplitude.
ii. The solution is stable at large values of the cubic velocity coefficient, and the amplitude of the controlled system decreases as it increases.
iii. A drop in the natural frequency ω causes the system's amplitude to decrease.
iv. The numerical results and the approximate solution of the controlled system agree very well.

In our future work, we can improve the behavior of this oscillator using other types of control, such as the positive position feedback and the PID controller with time-delay feedback. It is also possible to combine this oscillator with the cantilever beam and study the behavior of this new system.

Conflict of interest

The authors have no conflict of interest to declare.

Funding

The authors received no specific funding for this work.

Acknowledgments

The authors would like to extend their sincere appreciation to the editor and all reviewers for their valuable comments that improved the quality of this research.

Appendix

$$E_0(T_0,T_1,T_2)=(2\beta_2-\frac{13\alpha_1\alpha_3}{\omega^2}+2i\,\omega\alpha_2\alpha_3)A^2\bar{A}^2;$$

$$E_1(T_0,T_1,T_2)=\frac{-7.25A^3\bar{A}\alpha_1\alpha_2}{3\omega^2}-\frac{19i\omega A^3\bar{A}\alpha_2\alpha_3}{12}+\frac{2i\alpha_2D_1A^2}{9\omega}+\frac{4i\mu\alpha_2A^2}{9};$$

$$E_2(T_0,T_1,T_2)=\frac{3A^4\bar{A}\alpha_1^2}{32\omega^4}+\frac{3iA^4\bar{A}\alpha_1\alpha_3}{16\omega}+\frac{9\omega^2A^4\bar{A}\alpha_3^2}{32}+\frac{5\beta_3A^4\bar{A}}{8\omega^2}+\frac{3i\alpha_1D_1A^3}{32\omega^3}-\frac{9\alpha_3D_1A^3}{32}-\frac{i\Gamma\omega A^3}{8}-\frac{3i\alpha_1\mu A^3}{32\omega^2}-\frac{3\omega\alpha_3\mu A^3}{32}+\frac{A^3\alpha_2^2}{6}+\frac{i\beta_1\omega A^3}{8\omega}$$

$$E_3(T_0,T_1,T_2)=\frac{-1.75A^4\alpha_1\alpha_2}{15\omega^2}+\frac{11i\omega A^4\alpha_2\alpha_3}{60}-\frac{\beta_2A^4}{15}$$

$$E_4(T_0,T_1,T_2)=\frac{A^5\alpha_1^2}{84\omega^4}-\frac{iA^5\alpha_1\alpha_3}{16\omega}-\frac{3\omega^2A^5\alpha_3^2}{64}+\frac{\beta_3A^5}{24\omega^2}$$

$$,E_5(T_0,T_1,T_2)=\frac{f}{2(\omega^2-\Omega^2)}.$$

References

Amer, Y. A., Abd EL-Salam, M. N., & EL-Sayed, M. A. (2022). Behavior of a hybrid Rayleigh-Van der Pol-duffing oscillator with a PD controller. *Journal of applied research and technology*, *20*(1), 58-67. https://doi.org/10.22201/icat.24486736e.2022.20.1.1412

Amer, Y. A., El-Sayed, A. T., & Abd EL-Salam, M. N. (2020a). Outcomes of the NIPPF Controller Linked to a Hybrid Rayleigh–Van der Pol-Duffing Oscillator. *Journal of Control Engineering and Applied Informatics*, *22*(3), 33-41.

Amer, Y. A., El-Sayed, A. T., & Abd El-Salam, M. N. (2020b). Position and Velocity Time Delay for Suppression Vibrations of a Hybrid Rayleigh-Van der Pol-Duffing Oscillator. *Sound & Vibration*, *54*(3). https://doi.org/10.32604/sv.2020.08469

Barron, M. A. (2016). Stability of a ring of coupled van der Pol oscillators with non-uniform distribution of the coupling parameter. *Journal of applied research and technology*, *14*(1), 62-66. https://doi.org/10.1016/j.jart.2016.01.002

EL-Sayed, A. T. (2021). Resonance behavior in coupled Van der Pol harmonic oscillators with controllers and delayed feedback. *Journal of Vibration and Control*, *27*(9-10), 1155-1170. https://doi.org/10.1177/1077546320938182

Hamed, Y. S., Alotaibi, H., & El-Zahar, E. R. (2020). Nonlinear vibrations analysis and dynamic responses of a vertical conveyor system controlled by a proportional derivative controller. *IEEE Access*, *8*, 119082-119093. https://doi.org/10.1109/ACCESS.2020.3005377

Huang, C. (2018). Multiple scales scheme for bifurcation in a delayed extended van der Pol oscillator. *Physica A: Statistical Mechanics and its Applications*, *490*, 643-652. https://doi.org/10.1016/j.physa.2017.08.035

Kamel, M. M. (2009). Nonlinear behavior of Van der Pol oscillators under parametric and harmonic excitations. *Physica Scripta*, *79*(2), 025004. https://doi.org/10.1088/0031-8949/79/02/025004

Kandil, A., Hamed, Y. S., Abualnaja, K. M., Awrejcewicz, J., & Bednarek, M. (2022). 1/3 order subharmonic resonance control of a mass-damper-spring model via cubic-position negative-velocity feedback. *Symmetry*, *14*(4), 685. https://doi.org/10.3390/sym14040685

Kumar, P., Kumar, A., & Erlicher, S. (2017). A modified hybrid Van der Pol–Duffing–Rayleigh oscillator for modelling the lateral walking force on a rigid floor. *Physica D: Nonlinear Phenomena*, *358*, 1-14. https://doi.org/10.1016/j.physd.2017.07.008

Kumar, P., Kumar, A., Racic, V., & Erlicher, S. (2018). Modelling vertical human walking forces using self-sustained oscillator. *Mechanical Systems and Signal Processing*, *99*, 345-363. https://doi.org/10.1016/j.ymssp.2017.06.014

Kumar, P., Narayanan, S., & Gupta, S. (2016). Investigations on the bifurcation of a noisy Duffing–van der Pol oscillator. *Probabilistic Engineering Mechanics*, *45*, 70-86. https://doi.org/10.1016/j.probengmech.2016.03.003

Nayfeh, A. H. (1978). *Perturbation methods* (Vol. 8, Número 5, pp. 417-418). https://doi.org/10.1002/9783527617609

Sadeghi, S. A. M., Ebrahimpour, B., Bakhshinezhad, N., & Sadeghi, S. M. N. M. M. (2021). Analytical solution of nonlinear Van der Pol oscillator using a hybrid intelligent analytical inverse method. *Turkish Journal of Computer and Mathematics Education (TURCOMAT)*, *12*(13), 5614-5625.

Sayed, M., Elagan, S. K., Higazy, M., & Abd Elgafoor, M. S. (2018). Feedback control and stability of the Van der Pol equation subjected to external and parametric excitation forces. *International Journal of Applied Engineering Research*, *13*(6), 3772-3783.

Siewe, M. S., Kakmeni, F. M., Bowong, S., & Tchawoua, C. (2006). Non-linear response of a self-sustained electromechanical seismographs to fifth resonance excitations and chaos control. *Chaos, Solitons & Fractals*, *29*(2), 431-445. https://doi.org/10.1016/j.chaos.2005.08.210

Trueba, J. L., Baltanás, J. P., & Sanjuán, M. A. (2003). A generalized perturbed pendulum. *Chaos, Solitons & Fractals*, *15*(5), 911-924. https://doi.org/10.1016/S0960-0779(02)00210-2

Wang, W., Wang, X., Hua, X., Song, G., & Chen, Z. (2018). Vibration control of vortex-induced vibrations of a bridge deck by a single-side pounding tuned mass damper. *Engineering Structures*, *173*, 61-75. https://doi.org/10.1016/j.engstruct.2018.06.099